Catalysis Science & Technology

ROYAL SOCIETY OF CHEMISTRY

PAPER

Check for updates

Identifying and controlling the acid site distributions in mordenite zeolite for dimethyl ether carbonylation reaction by means of selective ion-exchange†

Shiping Liu, Hongchao Liu, Xiangang Ma, Yong Liu, Wenliang Zhu* and Zhongmin Liu (iD) *

As Brønsted acid sites in different types of channels exhibit distinct catalytic behaviors in the dimethyl ether (DME) carbonylation reaction over acidic mordenite (H-MOR) zeolites (*e.g.* acid sites in 8-membered ring channels for carbonylation reaction, acid sites in 12-membered ring channels for methanol-to-hydrocarbons reactions), the identification and regulation of acid site distribution in mordenite zeolites are of great importance to improve the catalytic performance. In this work, we employ the selective ion-exchange method to identify and control the acid site distribution in mordenite zeolites, and the chemical properties of acid sites in different channels are investigated by NH_3-TPD and CD_3CN FT-IR. Additionally, the effect of selective ion-exchange on the catalytic performance of DME carbonylation reaction is also discussed. The selective ion-exchange is realized by using tetramethylammonium (TMA^+) ions, which can selectively remove the counter ions in the 12-membered ring channels but are inaccessible to the counter ions in 8-membered ring channels due to the steric hindrance. The selective ion-exchange reveals that the relative amounts of acid sites in 12-membered ring channels and 8-membered ring channels are 68% and 32%, respectively. Interestingly, it is found that introducing TMA^+ into H-MOR zeolites significantly improves the catalytic activity and stability in DME carbonylation reaction as a result of depressing the methanol-to-hydrocarbons reactions. The 3TMA-H-MOR catalyst shows high stability for 210 hours on stream. The present work opens a new avenue for designing carbonylation catalysts with excellent stability in DME carbonylation reaction.

1. Introduction

Zeolite catalyzed dimethyl ether (DME) carbonylation provides a non-noble metal catalysis and halide-free process to produce high value-added methyl acetate, ethanol and acetic acid from carbon resources such as coal, nature gas, and renewable biomass, which has attracted much attention in recent years. Since this catalytic reaction was first reported by Iglesia and co-workers,[1] a number of zeolites including H-MOR, H-ZSM-35,[1,2] H-ZSM-5,[3] and H-EU-10 (ref. 4) have been extensively studied. Amongst these zeolites, the acidic MOR zeolite exhibits the highest carbonylation activity due to its unique framework structure. It is well known that MOR

National Engineering Laboratory for Methanol to Olefins, Dalian National Laboratory for Clean Energy, Dalian Institute of Chemical Physics, Chinese Academy of Sciences, Dalian, 116023, PR China. E-mail: wlzhu@dicp.ac.cn, liuzm@dicp.ac.cn

zeolites consist of two types of channels in *c* direction, namely 12-membered ring (12-MR) channel (6.5 × 7.0 Å) and compressed 8-membered ring (8-MR) channel (2.6 × 5.7 Å). These two types of channels are interconnected by the short 8-MR channels (4.8 × 3.4 Å) in *b* direction, which are typically referred to as side pockets.[5] Though all the channels have Brønsted acid sites (BAS), it has been demonstrated that the DME carbonylation reaction mainly occurs in the 8-MR channels due to the important confinement effect of 8-MR channels,[6–10] but the BAS in 12-MR channels can convert DME to hydrocarbons. As BAS in different types of pores play distinct roles in DME carbonylation reaction, determining and regulating the acid site distribution in mordenite zeolites are essential to establish the relationship between the acid sites and reactivity, which is very important to understand the catalytic principle and to improve the catalytic performance.

The locations of acid sites in mordenite zeolites have been intensively studied, and various techniques including neutron powder diffraction,[11] Fourier transform infrared (FT-IR) spectroscopy,[12–15] and solid-state magic angle spinning

This journal is © The Royal Society of Chemistry 2020

Catal. Sci. Technol., 2020, **10**, 4663–4672 | **4663**

nuclear magnetic resonance (MAS NMR)[16] have been applied to identify the acid site distribution in mordenite zeolites. For example, deconvolution of acidic OH stretching bands in FT-IR spectra into two peaks at ~3610 cm^{-1} and ~3585 cm^{-1} allows to quantitatively measure the amounts of acid sites in 12-MR and 8-MR channels, respectively. Using the IR method, however, the reported results are contradicting between authors. For example, Cherkasov *et al.*[13] reported that 29–32% of the BAS were located in the 8-MR channels, while Niwa *et al.*[14] obtained a high value of 64%, and Gounder *et al.*[17] showed 78% of BAS in the 8-MR channels. The discrepancy may be ascribed to the difference in the initial samples, however, the IR deconvolution is a kind of semi-quantitative method, and some errors introduced in the process of specimen handling and spectrum handling cannot be ignored.[13] Presently, there are still lacks of effective approaches for quantitatively characterizing the distributions of BAS in acidic mordenite zeolites.

In addition, another big problem with DME carbonylation reaction is that the mordenite zeolites suffer rapid deactivation due to coke formation. As the coke is evolved from the aromatic coke precursor molecules which can be accommodated in the large 12-MR channels but are sterically impeded in the 8-MR channels, it can be anticipated that removing the acid sites in 12-MR channels could improve the reaction stability. In this aspect, a number of approaches such as pre-adsorption of pyridine,[18] selective delamination,[19] and Zn–Cu ion-exchange[20] have been demonstrated, and the stability was improved to a certain extent, but challenges still remain. The difficulty in significantly enhancing the reaction stability is that the one-dimensional straight 12-MR channels in mordenite zeolites are very susceptible to pore plugging by the accumulation of coke species. Even small amounts of acid sites in 12-MR channels can lead to deactivation. Hence, in order to prolong the lifetime, the concentration of the acid sites in 12-MR channels must be reduced to a very low level, which requires developing new methods for controlling the distribution of BAS in the mordenite zeolites.

In the present work, we develop a novel strategy to determine and control the acid site distributions in mordenite zeolites through selective ion-exchange with tetramethylammonium (TMA) ions. The influence of introducing TMA$^+$ ions into mordenite zeolite on DME carbonylation reaction is also discussed. Additionally, the acidic properties of mordenite zeolites are investigated by using the probe molecules including NH$_3$ and d_3-acetonitrile (CD$_3$CN). The deactivation behavior of mordenite catalysts is also explored by analyzing the coke species retained in the spent catalysts. The insights shown in this work should be of great benefit to designing better mordenite catalysts for DME carbonylation reaction.

2. Experimental

2.1 Catalyst preparation

The parent MOR powder with a Si/Al ratio of 17 was purchased from Saint Chemical Materials. The as-received sample was calcined in air at 550 °C to remove the organic templates. After calcination, the sample was exchanged in 1.0 M NH$_4$NO$_3$ aqueous solution (10 mL of solution per g of zeolite) at 80 °C for 4 hours three times to remove the Na$^+$ ions. In the present work, the ratio of liquid volume to solid mass for ion-exchange was kept at 10 mL g^{-1} unless otherwise specified. The obtained NH$_4$-MOR sample was calcined in air at 550 °C for 4 hours to convert to H-type mordenite (denoted as H-MOR). H-MOR sample was exchanged with 1.0 M NaCl aqueous solution at 80 °C for 4 hours three times to ensure that all the protons were replaced by Na$^+$ ions. Then the exchanged sample was washed thoroughly by deionized water to remove the residual NaCl. XRF element analysis showed that the sodium content in the dry exchanged sample was 0.88 mmol g^{-1}, and the Na/Al molar ratio was close to 1, indicating that most of Na$^+$ ions were present as counter ions in the zeolites. The Na-MOR sample was then exchanged with 1.0 M tetramethylammonium chloride (TMACl) aqueous solution at 80 °C for 4 hours three times, followed by drying at 110 °C overnight. Then, the TMA-exchanged Na-MOR was calcined in air at 550 °C for 4 hours, and TMA$^+$ ions were thermally decomposed to form protons. The obtained sample was designated as 8Na-12H-MOR. H-MOR sample was exchanged in 1.0 M TMACl aqueous solution at 80 °C for 4 hours. After filtration, the exchanged samples were washed thoroughly by deionized water. The exchanged samples were named as xTMA-H-MOR (x = 1, 2 and 3, the exchange times). In addition, TEA-H-MOR was prepared by exchanging with tetraethylammonium (TEA$^+$) chloride once under the same condition as mentioned above.

2.2 Characterizations

The powder XRD pattern was recorded on a PANalytical X'Pert PRO X-ray diffractometer with Cu-Kα radiation (λ = 0.15418 nm), operating at 40 kV and 40 mA. The Si/Al ratio and Na contents of samples were determined with PhilipsMagix-601 X-ray fluorescence (XRF) spectrometer. The crystal morphology was observed using a scanning electron microscopy (Hitachi SU8020). The contents of organic compounds on zeolites were measured by SDT Q600 thermal analyzer from ambient temperature to 800 °C at a ramping rate of 10 °C min^{-1} in air atmosphere (100 mL min^{-1}). Nitrogen adsorption–desorption isotherms at −196 °C were obtained on a Micromeritics ASAP2020. Prior to the measurement, the samples were degassed at 250 °C under vacuum for 1 hour. BET model was used to estimate the surface areas of the samples. The pore volumes of samples were calculated by t-plot method. Temperature-programmed desorption of ammonia (NH$_3$-TPD) was measured on a Micrometric 2920 chemical adsorption instrument. Each sample (20–40 mesh, 0.20 g) was loaded into a quartz U-shaped reactor and pretreated at 350 °C for 1 hour in flowing He. After the pre-treatment, the sample was cooled to 150 °C and saturated with NH$_3$ gas. Then, NH$_3$-TPD was

4664 | *Catal. Sci. Technol.*, 2020, **10**, 4663–4672

This journal is © The Royal Society of Chemistry 2020

carried out in a constant flow of He (20 mL min^{-1}) from 100–700 °C at a heating rate of 10 °C min^{-1}.

Infrared spectra were recorded with a Bruker Tensor-27 FT-IR spectrometer at a resolution of 4 cm^{-1}. Self-supporting wafer of the solid (diameter 13 mm, 15–20 mg) was placed into an IR cell connected to a vacuum system. Then the sample was outgassed by heating to 350 °C with a ramping rate of 1 °C min^{-1} and keeping at 350 °C for 1 hour. Afterwards, the sample was cooled to room temperature, and the reference spectrum was recorded. For the adsorption of pyridine, the temperature again increased to 350 °C, and pyridine was introduced at this temperature and evacuated at the same temperature for 1 hour. Then, the sample was cooled to room temperature, and the spectra of pyridine adsorbed on zeolite were recorded. For the studies of d_3-acetonitrile (CD$_3$CN) adsorption, the sample was first outgassed at 350 °C for 1 hour under vacuum condition and subsequently exposed to the CD$_3$CN for 5 min after cooling down to room temperature. Then, desorption of CD$_3$CN was performed at 30, 50, 100, 150 and 200 °C for 10 min. Then, the sample was cooled to room temperature, and the IR spectra were collected.

2.3 DME carbonylation reaction test

The obtained MOR sample was pressed, sieved to 20–40 meshes. 1.0 g or 0.8 g catalyst was loaded in a fixed-bed stainless steel reactor with inner diameter of 10 mm. Prior to reaction, the catalyst was activated at 300 °C or 250 °C (for TMA-exchanged samples) in flowing nitrogen for 1 hour and then cooled to 200 °C. Then, a reactant gas mixture (5% DME, 35% CO, and 60% N$_2$) was introduced into the reactor, and the reaction pressure was raised to 2.0 MPa. The effluent products from reactor were analyzed by an online Agilent 7890B GC equipped with a PLOT-Q capillary column. DME conversion and product selectivities were calculated based on the carbon coming from DME:

$$Sel_{AcOH} = \left(\frac{AcOH_{outlet}}{2MA_{outlet} + MeOH_{outlet+outlet} + \sum_{1}^{n} nC_nH_{moutlet}} \right) \times 100\%$$

$$Sel_{C_nH_m} = \left(\frac{nC_nH_{moutlet}}{2MA_{outlet} + MeOH_{outlet+outlet} + \sum_{1}^{n} nC_nH_{moutlet}} \right) \times 100\%$$

DME$_{outlet}$, MA$_{outlet}$, MeOH$_{outlet}$, AcOH$_{outlet}$, DME$_{outlet}$, and C$_n$H$_{moutlet}$ stand for the relative molar concentrations of DME and products in outlet gas.

2.4 Analyzing the organic species retained in the zeolites with GC-MS

The spent catalysts were analyzed by thermogravimetric analysis (TGA), and the weight loss between 250–700 °C was used to estimate the coke contents. In order to identify the organic species confined in the pores of zeolites, the spent catalysts (50.0 mg) were dissolved in 1.0 ml 40% HF solution. The coke species were extracted with 1.0 ml CH$_2$Cl$_2$ with C$_2$Cl$_6$ (200 ppm) as interior label. After neutralization and separation, the CH$_2$Cl$_2$ solution was analyzed by a GC-MS equipped with a HP-5 capillary column and an FID detector.

3. Results and discussion

3.1 The relative amounts of Na$^+$ ions in 12-MR channels and 8-MR channels

The physicochemical properties of MOR samples used in this work are given in Fig. S1 and Table S1.† XRD pattern and SEM images of the sample reveal the pure MOR framework

$$X_{DME} = \left(1 - \frac{2DME_{outlet}}{2MA_{outlet} + MeOH_{outlet} + AcOH_{outlet} + \sum_{1}^{n} nC_nH_{moutlet} + 2DME_{outlet}} \right) \times 100\%$$

$$Sel_{MA} = \left(\frac{2MA_{outlet}}{2MA_{outlet} + MeOH_{outlet+outlet} + \sum_{1}^{n} nC_nH_{moutlet}} \right) \times 100\%$$

$$Sel_{MeOH} = \left(\frac{MeOH_{outlet}}{2MA_{outlet} + MeOH_{outlet+outlet} + \sum_{1}^{n} nC_nH_{moutlet}} \right) \times 100\%$$

without impurity phases. The BET surface area and external surface area are 393 m^2 g^{-1} and 36.9 m^2 g^{-1}, respectively, indicating that most of surface area is contributed by the micropore.

The relative amounts of Na$^+$ ions in 12-MR channels and 8-MR channels are determined through ion-exchange with NH$_4$NO$_3$ and TMACl. The ion-exchange results are shown in Fig. 1. It can be seen that the Na$^+$ exchange degree reaches 95% at the first step of exchanging with NH$_4$NO$_3$. Being exchanged with NH$_4$NO$_3$ twice, all the Na$^+$ ion in zeolites are removed. While, after three ion-exchange steps with TMACl, the maximum exchange degree reaches 68%, and 32% Na$^+$
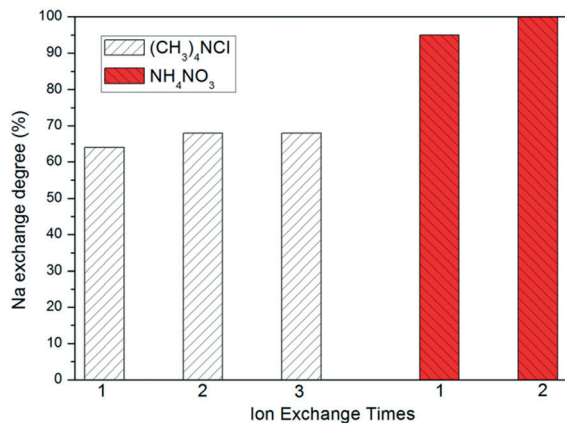
This journal is © The Royal Society of Chemistry 2020

Catal. Sci. Technol., 2020, **10**, 4663–4672 | **4665**

Fig. 1 The ion-exchange behaviors of Na-MOR sample with NH_4^+ and TMA^+ ions. Ion-exchange conditions: TMACl or NH_4NO_3 concentration in solution (1.0 M), temperature (80 °C), time (4 hours), volume of solution per g of zeolite (10 mL g^{-1}).

ion cannot be removed by TMA^+ ions. The difference in the maximum Na exchange degree between NH_4NO_3 and TMACl is resulted from the difference in the sizes of NH_4^+ and TMA^+ ions. The diameter of TMA^+ ions is about 6.4 Å,[21] which is between the pore openings of 8-MR channels and 12-MR channels and is much bigger than NH_4^+ ions. The small NH_4^+ ions can exchange with all the Na^+ ions in mordenite zeolites, while the large TMA^+ ions, in principle, only exchange with the Na^+ ions in 12-MR channels but not the Na^+ ions in 8-MR channels because of the steric hindrance. When the Na^+ ions levels no longer change with the exchange times, presumably, the Na^+ ions in the 12-MR channels are completely removed, and only Na^+ ions in 8-MR channels remain. Hence, on the basis of the above analysis, it can be initially deduced that 68% of Na^+ ions are located in 12-MR channels, and 32% of Na^+ ions situate in 8-MR channels. Both the Na^+ ions and protons are counter ions, and their locations are determined by the framework Al atoms. According to the Na^+ ions distribution in mordenite, we surmise that the ratio of the protons between the 12-MR channels and 8-MR channels is about 2:1, which is consistent with the works of Makarova[12] and Alberti.[15] In
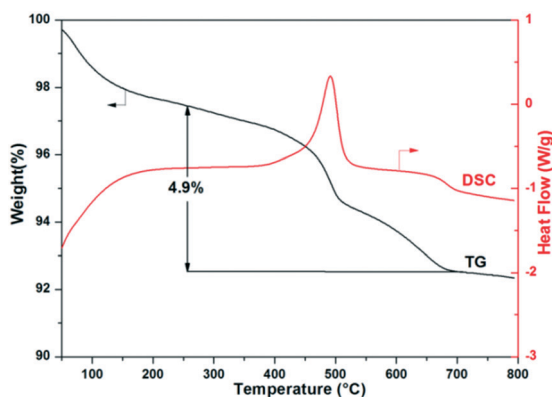
addition, the selective ion-exchange method is also employed to investigate the Na distribution of mordenite zeolite with a Si/Al of 9.8. Fig. S3† gives the Na exchange degrees as a function of ion-exchange times. After repeating three times, the maximum Na exchange degree is 62%, indicating that 62% of Na^+ ions are located in 12-MR channels. This result demonstrates that the selective ion-exchange method can be generally applied for determining the acid site distribution of mordenite with Si/Al ratios in the range of 9.8–17.

In order to investigate the state of TMA^+ ions in zeolites, thermal analysis for the TMA-exchanged Na-MOR sample is conducted. As illustrated in Fig. 2, the mass loss in the TG curve below 250 °C is due to the vaporing of adsorbed water. A weight change of 4.9% in the temperature range of 250–700 °C is observed, which is attributed to the combustion of TMA^+ ions evidenced by the large exothermic peak at 492 °C in the differential scanning calorimetry (DSC) curve. According to the weight loss, the molar content of TMA^+ ions in zeolite is estimated to be 0.63 mmol g^{-1}, which is very close to the content of Na^+ ions (0.6 mmol g^{-1}) expelled from the zeolites. Therefore, it can be inferred that the TMA^+ ions equimolarly substitute with Na^+ ions during the ion-exchange

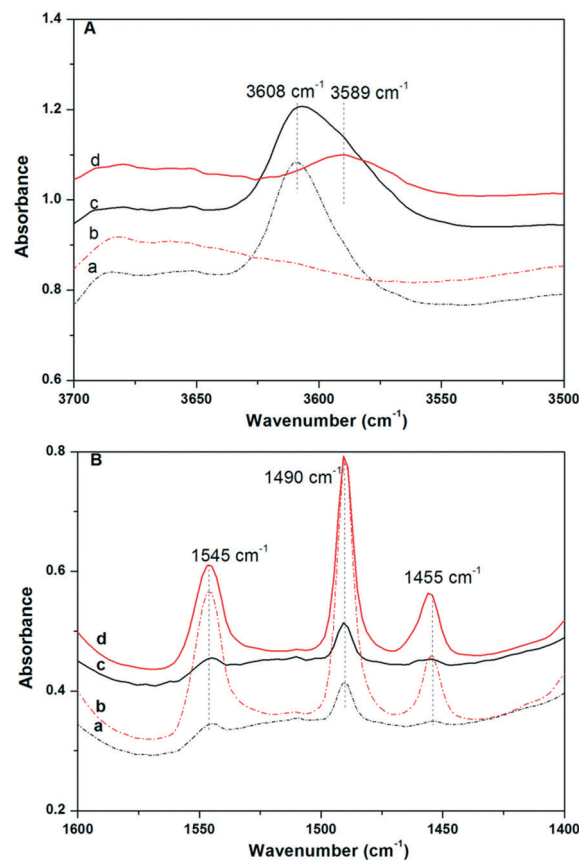**Fig. 2** Thermal analysis for TMA-exchanged Na-MOR sample.

Fig. 3 The spectra of H-MOR and 8Na-12H-MOR before and after adsorbing pyridine. (a) 8Na-12H-MOR, (b) 8Na-12H-MOR after adsorbing pyridine, (c) H-MOR, and (d) H-MOR after adsorbing pyridine. Pyridine introduced at 350 °C and evacuated at the same temperature. All the spectra were recorded at room temperature. A: The region of OH stretching frequencies, B: 1600–1400 cm^{-1} range.

4666 | *Catal. Sci. Technol.*, 2020, **10**, 4663–4672

This journal is © The Royal Society of Chemistry 2020

process and are present as counter ions compensating the negative charge of the zeolites. In order to confirm that TMA^+ ions have no access to the counter ions in 8-MR channels, we further investigate the acid site distributions of H-MOR and 8Na-12H-MOR samples by FT-IR method using pyridine as the probe molecule, and the IR spectra are shown in Fig. 3. After being dehydrated at 350 °C, an asymmetrical band at 3608 cm^{-1} with a shoulder peak at 3589 cm^{-1} is observed over H-MOR sample. It has been widely accepted that the bands 3608 cm^{-1} and 3589 cm^{-1} should be assigned to the bridging OH in 12-MR channels and 8-MR channels, respectively. After contacting with pyridine molecules, the strong peak at 3608 cm^{-1} disappears, while the small shoulder peak at 3589 cm^{-1} resists. The disappearance of OH stretching frequencies simultaneously gives rise to three peaks at 1545 cm^{-1}, 1490 cm^{-1}, and 1455 cm^{-1}, the characteristic bands of pyridine adsorbed on Brønsted and Lewis acid sites. Differing from the H-MOR sample, 8Na-12H-MOR sample displays a more symmetrical acidic OH stretching band at 3608 cm^{-1}, and the shoulder peak at 3589 cm^{-1} is not observed. Exposing to pyridine vapors results in a complete disappearance of the stretching band of the acidic OH group, indicating that there are no BAS in 8-MR channels. This result confirms that the Na^+ ions in 8-MR channels cannot be exchanged by TMA^+ ions. Moreover, the characteristic band of pyridine reacting Na^+ ions at 1443 cm^{-1} is not observed, confirming that the Na^+ ions in the 12-MR channels are completely removed. Additionally, the absence of acid sites in 8-MR channels also suggests that no Na^+ ions migrate from the 8-MR channels to 12-MR channels during the calcination process. Generally, the cations in the zeolite are mobile at high temperature and can migrate between different cation positions. A paradigmatic case[22] is that the Na^+ ions in the sodalite cages of FAU zeolites can migrate into the supercages during calcination process. If Na^+ ions migration occurs in the 8Na-12H-MOR sample, it would lead to the migration of protons from 12-MR channels to 8-MR channels. However, as illustrated by the IR spectra, there is no acid site in 8-MR channels. Hence, we can conclude that Na^+ ions still site in the 8-MR channels after calcination, and the acid sites are exclusively located in the 12-MR channels for the 8Na-12H-MOR sample.

3.2 The acid properties of mordenite zeolite

Through the aforementioned selective ion-exchange method, the samples with different distributions of acid site can be prepared, which provides an opportunity to explore the acid properties of BAS in 12-MR channels and 8-MR channels by the NH_3-TPD technique. As it is shown in Fig. 4, two NH_3 desorption peaks in the range of 150–323 °C and 323–700 °C, which correspond to the NH_3 desorption from weak and strong acid sites, respectively, are observed. The low-temperature peak (l-peak) of 8Na-12H-MOR sample shows a higher intensity because the residual Na^+ ions in the 8-MR channels act as Lewis acid sites. However, intensity of high-temperature peak (h-peak) of H-MOR sample is higher, indicating that H-MOR sample has more strong acid sites. The ratio of integral area of h-peak between 8Na-12H-MOR and H-MOR is 0.7, suggesting that BAS in 12-MR channels account for 70% of total acid sites in mordenite zeolites. This value is in line with the Na^+ ions distribution determined by the TMA-exchanged method (68% in 12-MR channels). By
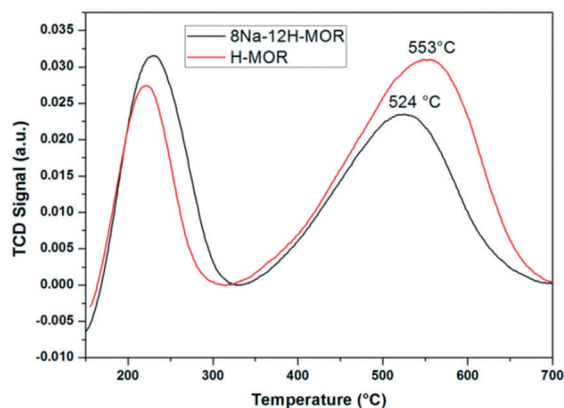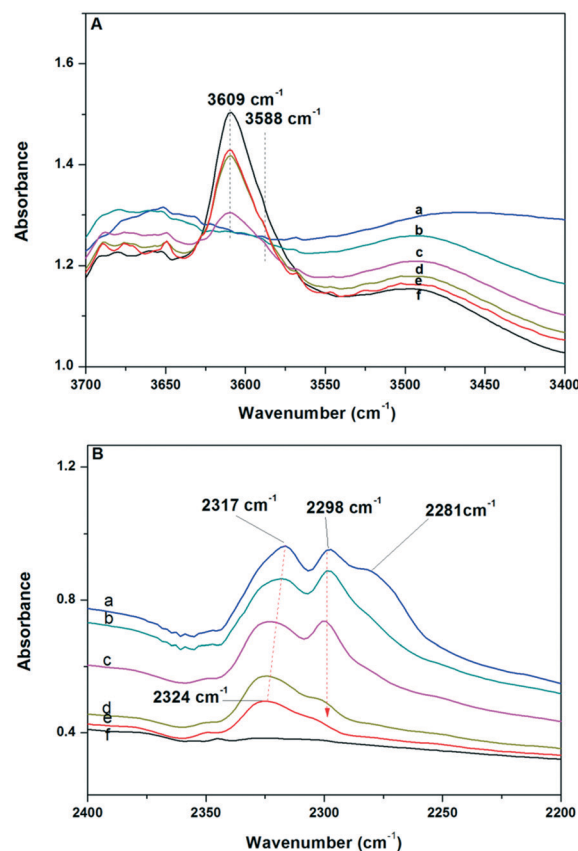

Fig. 5 FT-IR spectra of H-MOR before (f) and after (a) adsorbing CD_3-CN at room temperature. Then desorption of CD_3CN at (b) 50, (c) 100, (d) 150, and (e) 200 °C. All the spectra were recorded at room temperature. A: The region of OH stretching frequencies, B: the CN vibrational region.

Fig. 4 NH_3-TPD profiles of H-MOR and 8Na-12H-MOR.

This journal is © The Royal Society of Chemistry 2020

Catal. Sci. Technol., 2020, **10**, 4663–4672 | **4667**

comparing with the position of the maximum of the h-peak, it is found that H-MOR presents a higher desorption temperature. Considering that the difference in the acid site distributions in the two samples, the h-peak shifting towards higher desorption temperature is caused by the BAS in 8-MR channels. This means that the reaction between NH_4^+ cations and the framework in 8-MR channels is stronger than that in 12-MR channels, suggesting the special local environment of BAS in the 8-MR channels.

The acidic properties of mordenite zeolites are further investigated by FT-IR spectroscopy using the weak base CD_3CN as the probe molecule. The IR spectra of H-MOR sample before and after adsorbing CD_3CN are depicted in Fig. 5. Before the adsorption of CD_3CN, the bridging OH stretching bands at around 3609 cm^{-1} are observed. Introducing CD_3CN into the infrared cell, the acidic OH bands vanish, indicating that the small CD_3CN molecules are accessible to all the acid sites in the mordenite zeolites. The disappearance of OH bands is accompanied by the appearance of three bands at 2317 cm^{-1}, 2295 cm^{-1} and 2281 cm^{-1} in the C≡N stretching region,[23] which are assigned to CD_3CN bonded on the acid sites in 8-MR channels, the acid sites 12-MR channels and the terminal SiOH groups, respectively. It is known that the $\nu(C≡N)$ frequency correlates with the acid strength of acid sites, and stronger acid sites cause an upward shift of $\nu(C≡N)$ frequency.[24] Hence, it seems that the acid strength of BAS in 8-MR channel is higher than that in 12-MR channels. While Marie et al.[23] suggested that the higher $\nu(C≡N)$ frequency arises from the confinement effect of the constrained 8-MR channels. In the opinion of Jones and co-workers,[25] the intrinsic acid strength of BAS at different T positions is similar according to the calculated deprotonation energies, but the sizes of the confining voids near the acid sites are different, remarkably influencing the confinement effect on the guest species in the molecular size voids. The confinement effect can change some properties of acid sites such as vibrational frequency and NH_3 adsorption enthalpies,[26] which are frequently used as the indicators of the acid strength, but in fact, the higher NH_3 desorption temperature in 8-MR channels and the higher $\nu(C≡N)$ frequency[27] are likely ascribed to the confinement effect. For the carbonylation of DME, it was reported that the confinement effect of 8-MR channels plays a crucial role in stabilizing the ion-pair transition state of the rate-determining steps, hence promoting the carbonylation reaction. The acidic properties revealed by NH_3-TPD and CD_3-CN FT-IR methods are consistent with the reaction behaviors of DME carbonylation. Heating the sample to 50 °C leads to the disappearance of band at 2281 cm^{-1}. Further increasing the evacuation temperature to 100 °C, the intensities of bands at 2317 cm^{-1} and 2298 cm^{-1} decrease, and the $\nu(OH)$ band at 3609 cm^{-1} recovers to a small peak. When the evacuation temperature increases to 200 °C, the bands at 2298 cm^{-1} and 2317 cm^{-1} almost disappears completely, but a new band at 2324 cm^{-1} appears, which is due to CD_3CN adsorbed on Lewis acid sites.
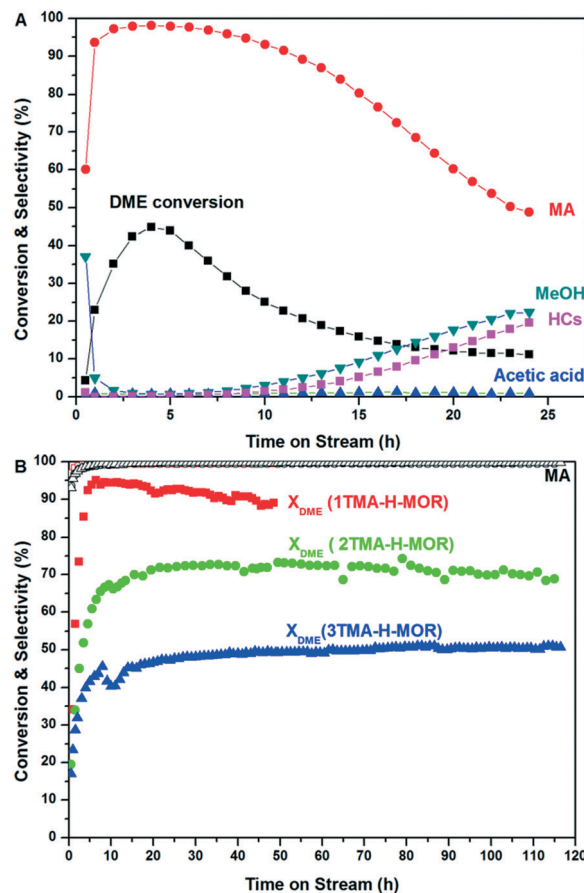

Fig. 6 The catalytic performance of DME carbonylation over H-MOR and TMA-exchanged H-MOR. Reaction condition: DME/CO/N$_2$ = 5/35/60, 200 °C, 2.0 MPa, A: GHSV = 1800 mL g$_{cat}$$^{-1}$ h^{-1}; B: GHSV = 2250 mL g$_{cat}$$^{-1}$ h^{-1}.

3.3 Selective removal of acidic sites in 12-MR channels

As it has been outlined above, TMA$^+$ ions selectively exchange with the Na$^+$ ions in 12-MR channels but are inaccessible to the Na$^+$ ions in 8-MR channels. Both Na$^+$ ions and protons are exchangeable counter ions. In principle, TMA$^+$ ions also have no access to the acid sites in 8-MR channels. This can be confirmed by the IR spectrum of TMA-exchanged H-MOR sample. As displayed in Fig. S4,† a small band at 3583 cm^{-1}, which should be assigned to the acid sites in 8-MR channels, can be observed, indicating that the acid sites in 8-MR channels cannot be removed by TMA$^+$ ions. Additionally, the XRD patterns of TMA-exchanged H-MOR samples are given in Fig. S5.† All the samples preserve the crystallinity after the ion-exchange, indicating that introduction of TMA$^+$ ions does not cause notable change of the framework structure. However, the catalytic performances over H-MOR and TMA-exchanged H-MOR are considerably different. It can be seen from Fig. 6A that the H-MOR sample shows a poor catalytic performance with a maximum DME conversion of 45%, and the DME conversion decreases quickly to 11% within 24 hours. The decrease of DME conversion is accompanied by the increase of hydrocarbons selectivity, indicating that MTH reactions are responsible for deactivation due to coke

4668 | *Catal. Sci. Technol.*, 2020, **10**, 4663–4672

This journal is © The Royal Society of Chemistry 2020

formation. In comparison with the H-MOR sample, the 1TMA-H-MOR catalyst shows a surprisingly high DME conversion of 95% even under the condition of higher gas hourly space velocity (GHSV). In general, the promoting effects on reactivity were observed by the loading of metal ions such as Co cations,[28] Cu cations,[29] and Zn cations,[20] which were ascribed to the activation of CO. In this work, we do not think that the TMA$^+$ cations are able to activate the CO molecules. Moreover, the TMA$^+$ cations are located in 12-MR channels, while the carbonylation reaction occurs in 8-MR channels. Considering the spatial distance between the reactive sites and TMA$^+$ ions, it seems unreasonable to ascribe the promoting effect to the activation of CO. The higher activity over 1TMA-H-MOR sample probably results from the suppression of MTH reactions by removing the acid sites in 12-MR channels. MTH reactions not only produce hydrocarbons but also yield water molecules. And the water was reported to be able to inhibit the carbonylation reaction by competitive adsorption on the acid sites in 8-MR channels.[10] In order to confirm this assumption, we further study the effect of water on the catalytic performance. The results are given in Fig. S6.† It can be seen that the DME conversion significantly decreases from 83.5% to 14.8% when a small amount of water (100 ppm) is added into the reaction stream. After removing the water, the DME conversion gradually recovers to initial value. In addition, it should be noted that only one-third of BAS in mordenite are involved in the carbonylation reaction. When the negative impact of MTH reactions on the carbonylation reaction are reduced, the acid sites in 8-MR channels indeed show high reactivity towards the carbonylation reaction, and the methyl acetate synthesis rate reaches 14.7 mol mol^{-1} H$^+$ h^{-1} over 1TMA-H-MOR catalyst. Typically, the activity of DME carbonylation reaction increases in parallel with the population of BAS in 8-MR channels.[7] Hence, if BAS in 8-MR channels can be enriched, for example, through the controllable zeolite synthesis, it can be expected that a higher activity can be achieved.

Introducing TMA$^+$ ions into 12-MR channels not only improves the activity but also enhances the stability in DME carbonylation reaction. The conversion of DME over 1TMA-H-MOR catalyst slightly decreases from 95% to 89% within 49 hours. The much better stability results from the selective removal of BAS in 12-MR channels by TMA$^+$ ions. According to the TG curve of 1TMA-H-MOR sample shown in Fig. S7,†

the weight mass of TMA$^+$ ions is about 4.4%. When TMA$^+$ ions completely remove Na$^+$ ions in 12-MR channel, the content of TMA ions is 4.9%. This means that about 89.8% of BAS in 12-MR channels in the 1TMA-H-MOR sample are replaced by TMA$^+$ ions. Although removing most of the BAS in 12-MR channels significantly promote stability in DME carbonylation reaction in comparison with the H-MOR sample, the residual acid sites in 12-MR channels still deactivate the catalysts slowly. In order to minimize BAS in 12-MR channels, the steps of H-MOR exchanging with TMACl should be increased. As illustrated in Fig. S7,† TMA$^+$ cations accumulate with the increase of the exchange times, implying the decrease of acid sites in 12-MR channels. And it can be found that the stability in DME carbonylation reaction presents a clear trend with the amounts of TMA$^+$ ions. After repeating ion-exchange three times, no deactivation is observed over the 3TMA-H-MOR sample within 117 hours. Even the stability test lasts for 210 hours, there is still no sign of deactivation (Fig. S8†). The excellent stability over 3TMA-H-MOR sample offers an indication that the amounts of BAS in 12-MR channel are reduced to a very low level. This result, in turn, reflects that TMA$^+$ ions can remove most of the counter ions 12-MR channels and confirms the validity of the selective ion-exchange method for determining the Na$^+$ ions distribution in mordenite. Though the stability is improved by the TMA$^+$ ions, increasing the loadings of TMA$^+$ ions is found to adversely affect the carbonylation activity. The methyl acetate synthesis rates decrease with increasing the ion-exchange steps. The negative influence of increasing the amounts of TMA$^+$ ions on the activity is associated with the change of the textual properties by the TMA$^+$ ions. Fig. S9† gives the nitrogen adsorption–desorption isotherms of H-MOR and TMA-exchanged H-MOR samples, and their corresponding textual parameters are listed in Table 1. Note that the BET surface area of 1TMA-H-MOR sample sharply decreases to 64 m^2 g^{-1}, and the micropore volume is just only 1/10 that of H-MOR sample, suggesting that introducing TMA$^+$ ions into the 12-MR channels results in the pore plugging. Fortunately, the critical diameters of DME (4.1 × 1.9 × 1.5 Å) and methyl acetate (5.3 × 1.9 × 3.1 Å) molecules are small.[30] When the amounts of TMA$^+$ ions in 12-MR channels are low, the negative effect of TMA$^+$ ions on the diffusion of reactants and products molecules is not obvious, which is evidenced by the high DME carbonylation activity. However, with the increase of amounts of TMA$^+$ ions in

Table 1 Textural properties and reaction results of H-MOR and TMA-exchanged MOR samples

Sample	H-MOR	1TMA-H-MOR	2TMA-H-MOR	3TMA-H-MOR
S_{BET} [m^2 g^{-1}]^a	402	64	46	39
V_{micro} [cm^3 g^{-1}]^b	0.16	0.016	0.007	0.005
Amounts of TMA$^+$ [mmol g^{-1}]^c	—	0.56	0.58	0.61
Amounts of BAS [mmol g^{-1}]	0.88^d	0.32^e	0.30^e	0.27^e
MA synthesis rates [mol mol^{-1} H$^+$ h^{-1})]	2.0	14.7	12.1	8.2

^{a} BET specific surface area. ^{b} Single-point pore volume at $P/P_0 = 0.975$. ^{c} Calculated from the weight loss in the temperature range of 250–700 °C. ^{d} Calculated from the Na content. ^{e} The amounts of BAS in H-MOR minus the amounts of TMA$^+$ ions.

This journal is © The Royal Society of Chemistry 2020

Catal. Sci. Technol., 2020, **10**, 4663–4672 | **4669**
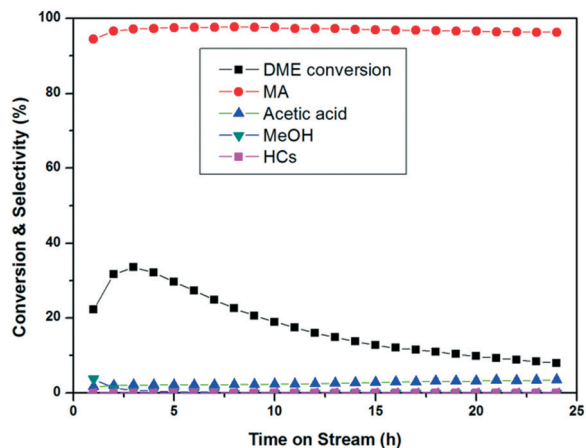
Fig. 7 The catalytic performance of TEA-H-MOR catalyst. Ion-exchange conditions: TEACl concentration in solution (1.0 M), temperature (80 °C), time (4 hours), volume of solution per g of zeolite (10 mL g^{-1}), reaction condition: DME/CO/N$_2$ = 5/35/60, 200 °C, 2.0 MPa, GHSV = 2250 mL g$_{cat}^{-1}$ h^{-1}.

zeolites, the BET surface areas and pore volumes further decrease, causing serious internal diffusion limitation. As a result, 2TMA-H-MOR and 3TMA-H-MOR show lower DME conversions compared with 1TMA-H-MOR.

We have demonstrated that the TMA$^+$ ions can selectively remove the protons in 12-MR channels and have a positive effect on the catalytic performance of DME carbonylation reaction. The advantage of using quaternary ammonium ions for ion-exchange is that there are a variety of organic ions with varying size. We further investigate the effect of the bigger quaternary ammonium ions (e.g. TEA$^+$ ions) on the catalytic performance of DME carbonylation reaction. And the reaction results over the TEA-exchanged sample are displayed in Fig. 7. In comparison with TMA-exchanged H-MOR sample, a much lower DME conversion and poorer stability are obtained. The worse catalytic performance is associated with the large diameter of TEA$^+$ ions. The bulky TEA$^+$ ions are subjected to a higher diffusion resistance when travelling in the 12-MR channels, rendering more acid sites

in the deep channels inaccessible to TEA$^+$ ions. Moreover, the bigger TEA$^+$ ion has a stronger pore-plugging effect than TMA$^+$ ion. Introducing TEA$^+$ ions into 12-MR channels can result in more serious diffusion limitation, as evidenced by the small specific surface area and pore volume (Fig. S10 and Table S2†). Therefore, exchanging with TEA$^+$ ions leads to an inferior catalytic performance.

3.4 The deactivation of mordenite catalyst in DME carbonylation reaction

The TG curves of the spent catalysts are shown in the Fig. 8. It can be seen that the spent H-MOR sample has the most coke contents. The combustion of cokes gives rise to two exothermic peaks in the DSC curves in the range of 250–400 °C and 400–650 °C, which correspond to the combustion of soft cokes and hard cokes.[31] The quantity of hard cokes is much more than that of soft cokes. Introducing TMA$^+$ ions into 12-MR channels can significantly reduce the coke contents (about 0.6 wt% on 1TMA-H-MOR-49h), especially the heavy cokes, clearly demonstrating the suppressive effect of TMA$^+$ ions on the coke formation. Meanwhile, the coke contents decrease with increasing the amounts of TMA$^+$ ions in the mordenite zeolites. The coke content over 3TMA-H-MOR sample almost can be neglected, in accordance with the excellent stability in DME carbonylation reaction. Furthermore, the confined coke species in the spent mordenite zeolite are analyzed by GC-MS technique. The result is displayed in Fig. 9. After the reaction for 24 hours, there are more than one hundred organic species in the spent H-MOR-24h sample. According to their structures, the coke species can be roughly divided into three categories: methyladamantanes, alkylbenzenes and alkylnaphthalenes. As suggested by Yuan and co-workers,[32] both of the methyladamantanes and alkylbenzenes derivatives have serious pore-plugging effect. Moreover, these compounds can further transform to the bigger alkylnaphthalenes derivatives during the reaction. Once the 12-MR channels are occupied
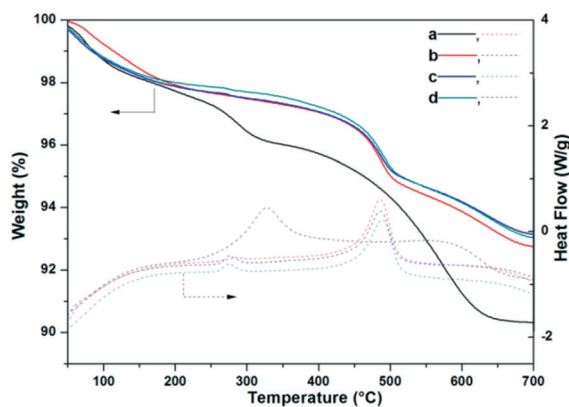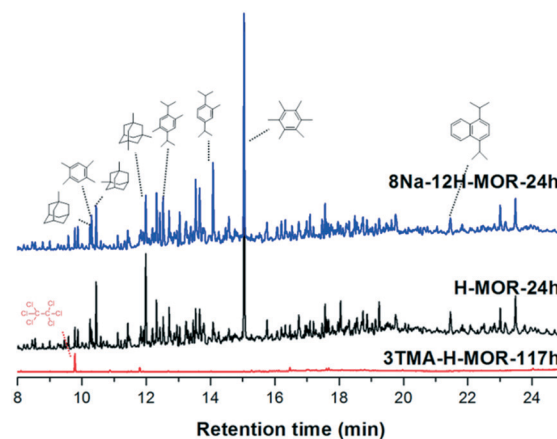

Fig. 8 Thermal analysis for the spent catalysts. Solid line = TG, dotted line = DSC. (a) H-MOR-24h, (b) 1TMA-H-MOR-49h, (c) 2TMA-H-MOR-115h, and (d) 3TMA-H-MOR-117h.

Fig. 9 GC-MS chromatograms of the organic species retained in the spent catalysts.

by the large coke molecules, there is no passage path for the reactants and products to diffuse into and out of the 8-MR channels,[33] resulting in deactivation. In contrast with the spent H-MOR-24h sample, only a few coke species with very low intensity are observed in the spent 3TMA-H-MOR-117h sample, directly demonstrating that the selective ion-exchange method is very effective to suppress coke formation. As for the DME carbonylation, the main product is methyl acetate, as proposed by Liu and co-workers,[34] which can act as coke precursors and contribute to the formation of the initial hydrocarbon pool species in the methanol-to-hydrocarbons reaction. In order to confirm whether the produced methyl acetate participates in the coke formation, the DME conversion over 8Na-12H-MOR sample is performed under the reaction conditions similar to the DME carbonylation reaction but in the absence of CO. After reaction for 24 hours, the spent catalyst is also analyzed by GC-MS. No marked difference in coke distribution between 8Na-12H-MOR-24h sample and H-MOR-24h sample is observed, implying that most of coke species in the mordenite originate from DME *via* the MTH reactions catalyzed by the BAS in 12-MR channels.

4. Conclusions

In summary, the acid sites distribution and acid properties of acid sites in acidic mordenite zeolites are studied systematically. The selective ion-exchange with the TMA$^+$ ions shows that 68% of Na$^+$ ions are located in 12-MR channels and 32% of Na$^+$ ions in the 8-MR channels, indicating that the ratio of protons in 12-MR channels to that in 8-MR channels is about 2 : 1. The selective removal of acid sites in 12-MR channels by exchanging with TMA$^+$ ions considerably promotes the catalytic performance of acidic mordenite zeolites for DME carbonylation reaction due to the suppression of MTH reactions. Particularly, a great enhancement of the stability in DME carbonylation is achieved over 3TMA-H-MOR catalyst, and no obvious deactivation is observed in the long-term stability test up to 210 hours. The combination of NH$_3$-TPD and CD$_3$CN FT-IR analysis confirms the special confinement effect of the 8-MR channels, which is beneficial to the DME carbonylation reaction. Differing from the TMA$^+$ ions, exchanging with TEA$^+$ ions leads to an inferior catalytic performance. Furthermore, the analysis from the TG and GC-MS demonstrates that the coke formation mainly originates from the DME rather than the methyl acetate *via* the MTH reactions in 12-MR channel, and the presence of TMA$^+$ ions can effectively suppress the formation of coke species. Our findings will contribute to the understanding of the acidic properties of mordenite zeolites. More importantly, it offers a direction for designing a mordenite catalyst with excellent performance in DME carbonylation reaction by controlling the acid sites distribution, for example, *via* controllable zeolites synthesis and selectively removing the acid sites in 12-MR channels.

Conflicts of interest

There are no conflicts to declare.

Acknowledgements

Notes and references

1 P. Cheung, A. Bhan, G. J. Sunley and E. Iglesia, *Angew. Chem., Int. Ed.*, 2006, **45**, 1617–1620.
2 X. Li, X. Liu, S. Liu, S. Xie, X. Zhu, F. Chen and L. Xu, *RSC Adv.*, 2013, **3**, 16549–16557.
3 S. Wang, S. Y. Li, L. Zhang, Z. F. Qin, Y. Y. Chen, M. Dong, J. F. Li, W. B. Fan and J. G. Wang, *Catal. Sci. Technol.*, 2018, **8**, 3193–3204.
4 X. B. Feng, J. Yao, H. J. Li, Y. Fang, Y. Yoneyama, G. H. Yang and N. Tsubaki, *Chem. Commun.*, 2019, **55**, 1048–1051.
5 P. Simoncic and T. Armbruster, *Am. Mineral.*, 2004, **89**, 421–431.
6 R. Gounder and E. Iglesia, *Chem. Commun.*, 2013, **49**, 3491–3509.
7 A. Bhan, A. D. Allian, G. J. Sunley, D. J. Law and E. Iglesia, *J. Am. Chem. Soc.*, 2007, **129**, 4919–4924.
8 A. Bhan and E. Iglesia, *Acc. Chem. Res.*, 2008, **41**, 559–567.
9 M. Boronat, C. Martinez-Sanchez, D. Law and A. Corma, *J. Am. Chem. Soc.*, 2008, **130**, 16316–16323.
10 M. Boronat, C. Martínez and A. Corma, *Phys. Chem. Chem. Phys.*, 2011, **13**, 2603.
11 A. Martucci, G. Cruciani, A. Alberti, C. Ritter, P. Ciambelli and M. Rapacciuolo, *Microporous Mesoporous Mater.*, 2000, **35-36**, 405–412.
12 M. A. Makarova, A. E. Wilson, B. J. van Liemt, C. M. A. M. Mesters, A. W. de Winter and C. Williams, *J. Catal.*, 1997, **172**, 170–177.
13 N. Cherkasov, T. Vazhnova and D. B. Lukyanov, *Vib. Spectrosc.*, 2016, **83**, 170–179.
14 M. Niwa, K. Suzuki, N. Katada, T. Kanougi and T. Atoguchi, *J. Phys. Chem. B*, 2005, **109**, 18749–18757.
15 A. Alberti, *Zeolites*, 1997, **19**, 411–415.
16 H. Huo, L. M. Peng, Z. H. Gan and C. P. Grey, *J. Am. Chem. Soc.*, 2012, **134**, 9708–9720.
17 R. Gounder and E. Iglesia, *J. Am. Chem. Soc.*, 2009, **131**, 1958–1971.
18 J. Liu, H. Xue, X. Huang, P. Wu, S. Huang, S. Liu and W. Shen, *Chin. J. Catal.*, 2010, **31**, 729–738.
19 H. F. Xue, X. M. Huang, E. S. Zhan, M. Ma and W. J. Shen, *Catal. Commun.*, 2013, **37**, 75–79.
20 A. A. C. Reule and N. Semagina, *ACS Catal.*, 2016, **6**, 4972–4975.
21 S. Lawton, M. E. Leonowicz, R. Partridge, P. Chu and M. K. Rubin, *Microporous Mesoporous Mater.*, 1998, **23**, 109–117.

This journal is © The Royal Society of Chemistry 2020

Catal. Sci. Technol., 2020, **10**, 4663–4672 | **4671**

22 P. Norby, F. I. Poshni, A. F. Gualtieri, J. C. Hanson and C. P. Grey, *J. Phys. Chem. B*, 1998, **102**, 839–856.

23 O. Marie, F. Thibault-Starzyk and J. C. Lavalley, *Phys. Chem. Chem. Phys.*, 2000, **2**, 5341–5349.

24 C. Paze, G. T. Palomino and A. Zecchina, *Catal. Lett.*, 1999, **60**, 139–143.

25 A. J. Jones and E. Iglesia, *ACS Catal.*, 2015, **5**, 5741–5755.

26 C. Lee, D. J. Parrillo, R. J. Gorte and W. E. Farneth, *J. Am. Chem. Soc.*, 1996, **118**, 3262–3268.

27 A. Simperler, R. G. Bell, M. D. Foster, A. E. Gray, D. W. Lewis and M. W. Anderson, *J. Phys. Chem. B*, 2004, **108**, 7152–7161.

28 M. Ma, E. S. Zhan, X. M. Huang, N. Ta, Z. P. Xiong, L. Y. Bai and W. J. Shen, *Catal. Sci. Technol.*, 2018, **8**, 2124–2130.

29 T. Blasco, M. Boronat, P. Concepción, A. Corma, D. Law and J. A. Vidal-Moya, *Angew. Chem., Int. Ed.*, 2007, **46**, 3938–3941.

30 A. A. C. Reule, *PhD thesis*, University of Alberta, 2016.

31 J. Liu, H. Xue, X. Huang, Y. Li and W. Shen, *Catal. Lett.*, 2010, **139**, 33–37.

32 C. Y. Yuan, Y. X. Wei, J. Z. Li, S. T. Xu, J. R. Chen, Y. Zhou, Q. T. Wang, L. Xu and Z. M. Liu, *Chin. J. Catal.*, 2012, **33**(2), 367–374.

33 T. He, X. C. Liu, S. T. Xu, X. W. Han, X. L. Pan, G. J. Hou and X. H. Bao, *J. Phys. Chem. C*, 2016, **120**, 22526–22531.

34 Y. Liu, S. Muller, D. Berger, J. Jelic, K. Reuter, M. Tonigold, M. Sanchez-Sanchez and J. A. Lercher, *Angew. Chem., Int. Ed.*, 2016, **55**, 5723–5726.